RESEARCH ARTICLE

[1]Key Laboratory of Luminescence and Optical Information, Ministry of Education, Beijing Jiaotong University, Beijing 100044, China; [2]Department of Chemistry, The Hong Kong University of Science and Technology, Hong Kong, China; [3]Institute of Polymer Optoelectronic Materials and Devices, State Key Laboratory of Luminescent Materials and Devices, South China University of Technology, Guangzhou 510640, China; [4]Organic Optoelectronic Materials Laboratory, Department of Chemistry, College of Science, Korea University, Seoul 02841, South Korea and [5]Center for Advanced Low-Dimension Materials, State Key Laboratory for Modification of Chemical Fibers and Polymer Materials, College of Materials Science and Engineering, Donghua University, Shanghai 201620, China

MATERIALS SCIENCE

Special Topic: Advanced Materials for Solar Energy Conversion

Approaching 18% efficiency of ternary organic photovoltaics with wide bandgap polymer donor and well compatible Y6 : Y6-1O as acceptor

Xiaoling Ma[1,†], Anping Zeng[2,†], Jinhua Gao[1], Zhenghao Hu[1], Chunyu Xu[1], Jae Hoon Son[4], Sang Young Jeong[4], Caixia Zhang[1], Mengyang Li[5], Kai Wang[1], He Yan[2,3], Zaifei Ma[5], Yongsheng Wang[1], Han Young Woo[4,*] and Fujun Zhang[1,*]

Corresponding authors. E-mails:
fjzhang@bjtu.edu.cn;
hywoo@korea.ac.kr
[†]Equally contributed to this work.

ABSTRACT

A series of ternary organic photovoltaics (OPVs) are fabricated with one wide bandgap polymer D18-Cl as donor, and well compatible Y6 and Y6-1O as acceptor. The open-circuit-voltage (V_{OC}) of ternary OPVs is monotonously increased along with the incorporation of Y6-1O, indicating that the alloy state should be formed between Y6 and Y6-1O due to their excellent compatibility. The energy loss can be minimized by incorporating Y6-1O, leading to the V_{OC} improvement of ternary OPVs. By finely adjusting the Y6-1O content, a power conversion efficiency of 17.91% is achieved in the optimal ternary OPVs with 30 wt% Y6-1O in acceptors, resulting from synchronously improved short-circuit-current density (J_{SC}) of 25.87 mA cm^{-2}, fill factor (FF) of 76.92% and V_{OC} of 0.900 V in comparison with those of D18-Cl : Y6 binary OPVs. The J_{SC} and FF improvement of ternary OPVs should be ascribed to comprehensively optimal photon harvesting, exciton dissociation and charge transport in ternary active layers. The more efficient charge separation and transport process in ternary active layers can be confirmed by the magneto-photocurrent and impedance spectroscopy experimental results, respectively. This work provides new insight into constructing highly efficient ternary OPVs with well compatible Y6 and its derivative as acceptor.

Keywords: organic photovoltaics, power conversion efficiency, ternary strategy, photon harvesting, morphology regulation

INTRODUCTION

In recent years, remarkable progress has been made on single junction organic photovoltaics (OPVs) due to the flourishing development of materials and device engineering, leading to over 17% power conversion efficiency (PCE) [1–4]. The organic semiconductor materials usually possess relatively narrow absorption spectra with the full-width at half-maximum less than 150 nm, resulting in limited photon harvesting in traditional binary active layers. Ternary OPVs have been established to improve photon harvesting of active layers as much as possible by integrating two donors/one acceptor or one donor/two acceptors with complementary absorp-tion spectra into one active layer. In fact, it is dubious to warrant performance improvement of ternary OPVs by taking the selection rule simply based on the absorption spectral complementarity among the used materials. Charge traps are ineluctably introduced in ternary active layers due to the different lowest-unoccupied-molecular-orbital (LUMO) energy levels between two acceptors or the distinct highest-occupied-molecular-orbital (HOMO) energy levels between two donors. The energy levels of the used materials should be considered to prevent forming deep charge traps in ternary active layers. Meanwhile, the incorporation of a third component with appropriate energy levels can help

achieve relatively high open-circuit-voltage (V_{OC}) in comparison with the host binary system, resulting in minimized energy loss (E_{loss}) of OPVs. It should be kept in mind that morphology optimization of active layers is a major challenge for the preparation of efficient ternary OPVs because of their distinct chemical and physical properties. The good material compatibility should provide larger potential to subtly adjust the phase separation degree of active layers, where the third component will take a critical role as morphology regulator. The optical bandgap, energy level and compatibility among the used materials should be comprehensively deliberated to develop efficient ternary OPVs. The appropriate third component can usually play multiple roles in the performance improvement of OPVs, such as improving photon harvesting [5,6], modifying molecular crystallinity [7], minimizing energy loss [8–10], adjusting photogenerated exciton distribution [11], and ameliorating phase separation degree for efficient exciton dissociation and charge transport [12–14]. Nowadays, most of the representative efficient OPVs were fabricated with Y6 or its derivatives as acceptor, which possess a novel A-DA′D-A structure with relatively low bandgap. The outstanding efficiencies of Y6 or its derivative-based OPVs should be mainly attributed to their wide and high photoresponsivity with relatively low E_{loss} (0.5–0.6 eV) [15–18]. The Y6 derivatives are usually designed and synthesized by slightly tailoring the function groups of Y6, resulting in slightly varied optical bandgap and energy level, as well as good compatibility with Y6. The well compatible Y6 and its derivatives may prefer to form an alloyed state for efficient electron transport in ternary active layers. The superiorities of Y6 and its derivatives may be simultaneously combined into one cell by employing their blends as acceptor. Highly ternary OPVs based on Y6 and its derivatives as acceptors are still rarely reported. In this work, a PCE of 17.91% is achieved in ternary OPVs with Y6 : Y6-1O as acceptor and wide bandgap polymer D18-Cl as donor. The PCE of 17.91% should be among the highest values of all ternary OPVs.

The chemical structures of D18-Cl, Y6 and Y6-1O are exhibited in Fig. S1a. The similar chemical structures of Y6 and Y6-1O suggest their good compatibility, which is beneficial in forming an alloy state for efficient electron transport in active layers. The absorption spectra of neat films and blend films were measured and are shown in Fig. S1b and c, respectively. The characteristic absorption peaks of D18-Cl, Y6 and Y6-1O are located at ~575, ~830 and ~800 nm, respectively. The photon harvesting of ternary blend films is gradually increased in the short wavelength range and decreased in the long wavelength range along with Y6-1O incorporation, which can be well explained by the absorption spectra of corresponding neat films. The well optimal photon harvesting of ternary blend films should be achieved by adjusting the Y6-1O content. All binary and ternary OPVs were fabricated with a conventional configuration of ITO/PEDOT:PSS/Active layer/PDIN/Al. The upside-down solvent vapor annealing treatment was employed with carbon disulfide for 20 s on active layers to optimize the phase separation degree. The detailed experimental procedure is described in the Supporting Information. The 17.07% PCE is achieved in D18-Cl : Y6 binary OPVs, which is larger than that of 15.44% for D18-Cl : Y6-1O binary OPVs. The Y6-1O binary OPVs exhibit a relatively large V_{OC} of 0.929 V compared with that of 0.881 V for D18-Cl : Y6 binary OPVs, which helps to improve the V_{OC}s of ternary OPVs. The PCE of ternary OPVs arrives at 17.91% by incorporating 30 wt% Y6-1O, resulting from a simultaneously improved short-circuit current-density (J_{SC}) of 25.87 mA cm^{-2}, fill factor (FF) of 76.92% and V_{OC} of 0.900 V compared with those of D18-Cl : Y6 binary OPVs. The performance improvement of ternary OPVs should be attributed to enhanced photon harvesting, minimized energy loss and improved active layer morphology for efficient exciton dissociation and charge transport in ternary active layers. This work may provide a new viewpoint for fabricating highly efficient ternary OPVs based on well compatible non-fullerene materials as acceptor.

RESULTS AND DISCUSSION

The current-density versus voltage ($J - V$) curves of all OPVs were measured under AM 1.5G simulated solar light with 100 mW cm^{-2} intensity, as exhibited in Fig. 1a. Based on the $J - V$ curves, key photovoltaic parameters of all OPVs are summarized in Table 1. The D18-Cl : Y6-based OPVs exhibit a PCE of 17.07% with a J_{SC} of 25.53 mA cm^{-2}, an FF of 75.88% and a V_{OC} of 0.881 V. The D18-Cl : Y6-1O-based OPVs exhibit a PCE of 15.44% with a J_{SC} of 22.72 mA cm^{-2}, an FF of 73.14% and a V_{OC} of 0.929 V. Both binary OPVs exhibit the FFs more than 73%, indicating that an efficient charge transport channel should be formed in two kinds of active layers. Meanwhile, there is apparent complementarity between J_{SC}s and V_{OC}s of two binary OPVs. The J_{SC} of D18-Cl : Y6 binary OPVs is much higher than that of Y6-1O-based binary OPVs, and the V_{OC} of D18-Cl : Y6-1O binary OPVs is much higher than that of Y6-based binary OPVs. The superiorities of two binary OPVs may be combined into one cell by employing Y6 : Y6-X as acceptor. Series of ternary OPVs were prepared by adjusting the

Figure 1. (a) The $J − V$ curves of typical OPVs with different Y6-1O content. (b) EQE spectra of the corresponding OPVs. (c) The reflection spectra of corresponding OPVs and the special device. (d) Absorption spectra of active layers in corresponding OPVs.

925.9 Ω cm^2 were simultaneously obtained for the OPVs with 30 wt% Y6-1O in acceptors, which are responsible for the highest FF of the optimal ternary OPVs.

To clarify the contribution of Y6-1O on performance improvement, the external quantum efficiency (EQE) spectra of OPVs were measured and are shown in Fig. 1b. It is apparent that EQE values of the optimal ternary OPVs can be improved in the short wavelength range from 370 to 630 nm, which may be mainly caused by well-balanced photon harvesting, exciton dissociation, charge transport and collection. The EQE values in the long wavelength range are gradually decreased along with the incorporation of Y6-1O, which can be reasonably explained by the relatively low EQE spectra of D18-Cl : Y6-1O binary OPVs. For a better understanding of the variation of EQE spectra dependence on Y6-1O content in acceptors, the absorption spectra of the active layers in real cells were investigated according to the reflection spectra of corresponding cells. The reflection spectra and absorption spectra of corresponding cells are shown in Fig. 1c and d, respectively. A special device with a structure of ITO/PEDOT:PSS/PMMA/PDIN/Al was fabricated to eliminate the effect of parasitic absorption in cells. The light absorption of glass/ITO substrate and interfacial layers can be obtained from this special device due to the negligible absorption of poly(methylmethacrylate) (PMMA) in the whole wavelength range. The absorption spectra of active layers in cells can be calculated by subtracting the parasitic absorption from the total absorption in OPVs. The detailed calculation process is described in the Supporting Information. The absorption spectra of the active layers in cells can really reflect the contribution of the third component to the photon harvesting of ternary active layers by considering the interference effect between the incident light and the reflected light from the Al electrode. The slightly decreased EQE values of the optimal ternary OPVs in the long wavelength range should be ascribed to decreased photon harvesting of ternary active layers. The photon harvesting of optimal ternary active layers

content of Y6-1O in acceptors. A PCE of 17.91% is achieved in the optimal ternary OPVs with 30 wt% Y6-1O, resulting from a simultaneously improved J_{SC} of 25.87 mA cm^{-2}, FF of 76.92% and V_{OC} of 0.900 V in comparison with those of D18-Cl : Y6 binary OPVs. The PCE of 17.91% is among the highest values for ternary OPVs. It should be highlighted that the 16.74% PCE and 76.07% FF can still be obtained in the ternary OPVs with 50 wt% Y6-1O in acceptors, indicating the excellent tolerance between Y6 and Y6-1O for fabricating efficient ternary OPVs. To better understand FF variation of ternary OPVs dependence on Y6-1O content in acceptors, the series resistance (R_S) and shunt resistance (R_{SH}) were calculated according to $J − V$ curves of OPVs, as summarized in Table 1. The R_Ss of OPVs show a decreased and then increased trend along with the increase of Y6-1O content, and the R_{SH}s of OPVs exhibit an opposite trend compared with R_Ss. The minimum R_S of 2.54 Ω cm^2 and maximum R_{SH} of

Table 1. Key photovoltaic parameters of all OPVs with different Y6-1O content.

Y6-1O content (wt%)	J_{SC} (mA cm^{-2})	V_{OC} (V)	FF (%)	PCE (Ave. ± Dev.[a]) (%)	R_S (Ω cm^2)	R_{SH} (Ω cm^2)
0	25.53	0.881	75.88	17.07 (16.86 ± 0.21)	2.91	841.8
15	25.89	0.889	76.27	17.55 (17.37 ± 0.23)	2.69	863.6
30	25.87	0.900	76.92	17.91 (17.83 ± 0.21)	2.54	925.9
50	24.16	0.911	76.07	16.74 (16.49 ± 0.27)	2.87	881.8
100	22.72	0.929	73.14	15.44 (15.26 ± 0.19)	3.16	626.0

[a]Average and deviation (Ave. ± Dev.) of PCEs were calculated with 10 individual cells from different batches.
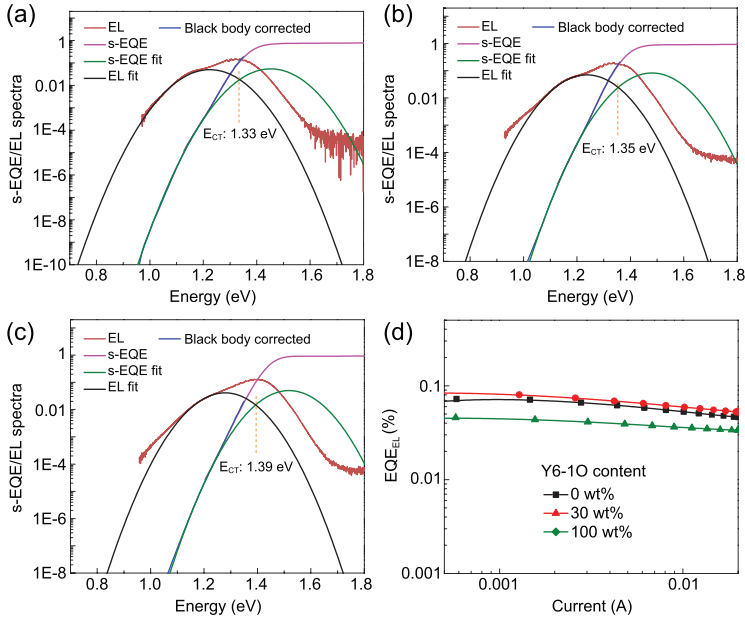
Figure 2. The s-EQE and EL spectra of (a) D18-Cl : Y6, (b) the optimal ternary and (c) D18-Cl : Y6-1O-based OPVs. (d) The EQE_{EL} spectra of typical binary and ternary OPVs.

is enhanced in the short wavelength range from 370 to 630 nm compared with that of binary active layers, which may be attributed to the more ordered molecular arrangement of D18-Cl and Y6 in ternary active layers with appropriate Y6-1O incorporation. The Y6-1O may act as morphology regulator to adjust molecular arrangement of D18-Cl and Y6 in ternary active layers.

To further investigate the reasons behind the performance improvement by incorporating Y6-1O, the detailed E_{loss} of OPVs was investigated. The E_{loss} of OPVs can be calculated according to the equation: $E_{loss} = E_g - eV_{OC}$, in which the bandgap (E_g) can be estimated according to the intersection between the normalized emission and absorption spectra of the acceptor films [19], as shown in Fig. S2. The total E_{loss} of OPVs can be divided into three parts, as described in the following equation:

$$E_{loss} = E_g - eV_{OC} = \Delta E_1 + \Delta E_2 + \Delta E_3$$
$$= \left(E_g - eV_{OC}^{SQ}\right) + \left(eV_{OC}^{SQ} - eV_{OC}^{Rad}\right)$$
$$+ \left(eV_{OC}^{Rad} - eV_{OC}\right).$$

Here, ΔE_1, ΔE_2 and ΔE_3 represent unavoidable radiative recombination loss above the bandgap, radiative recombination loss below the bandgap and non-radiative recombination loss, respectively. V_{OC}^{SQ} and V_{OC}^{Rad} are voltages in Shockley-Queisser limit and radiative limit, respectively [20]. The highly sensitive EQE (s-EQE) spectra and electroluminescence (EL) spectra were measured to evaluate the specific E_{loss} of OPVs, as shown in Fig. 2a–c. V_{OC}^{SQ}

is determined by E_{CT}/q, where E_{CT} represents the energy of charge transfer state. E_{CT} can be estimated by fitting the lower energy part of s-EQE spectra and higher energy part of EL spectra based on Marcus theory. According to the E_{CT} values, the V_{OC}^{SQ} is calculated to be 1.072, 1.090 and 1.128 V, corresponding to ΔE_1 of 0.383, 0.367 and 0.359 eV for D18-Cl : Y6, the optimal ternary- and D18-Cl : Y6-1O-based OPVs, respectively. The ΔE_1 of the optimal ternary OPVs is lower than that of D18-Cl : Y6-based binary OPVs, which contributes the performance improvement of ternary OPVs. The V_{OC}^{Rad} can be obtained according to the following equation:

$$qV_{OC}^{Rad} = KTln\left(\frac{J_{ph}(V_{oc})}{J_{0,rad}} + 1\right).$$

Here, $J_{0,rad}$ is the saturation current density calculated by considering only the blackbody radiation of the cell with the real absorption profile. K, T and q represent Boltzmann's constant, temperature of the sample and elementary charge, respectively. $J_{ph}(V_{oc})$ is the photocurrent at open-circuit condition [21]. The calculated ΔE_2 of optimal ternary OPVs is slightly increased compared with binary OPVs, as summarized in Table S1. ΔE_3 is linearly related to the natural logarithm of EQE_{EL}, as described by $\Delta E_3 = -KTln(EQE_{EL})$. As shown in Fig. 2d, the optimized ternary OPVs show higher EQE_{EL} of 9.96×10^{-4} than that of two binary OPVs, leading to the reduced non-radiative loss of 0.175 eV. The total E_{loss} can be obtained according to the sum of ΔE_1, ΔE_2 and ΔE_3. The E_{loss} of optimal ternary OPVs is 0.582 eV, which is lower than that of 0.597 eV in D18-Cl : Y6-based binary OPVs. The reduced E_{loss} by incorporating Y6-1O should play a vital role in the performance improvement of ternary OPVs.

For the OPVs with the same interfacial layers and electrodes, the V_{OC} strongly depends on the energy level difference between the donor's HOMO and acceptor's LUMO. The photogenerated holes will be transported along the channels formed by D18-Cl with the constant HOMO energy level. The V_{OC}s of ternary OPVs are monotonously increased along with Y6-1O incorporation, which should be ascribed to the gradually evaluated LUMO energy levels of an alloyed state of Y6 : Y6-1O [22,23]. To evaluate the compatibility of the used materials, the contact angles measurement of neat D18-Cl, Y6 and Y6-1O films were carried out based on liquid drops of water and methylene iodide, as shown in Fig. 3a. According to Wu's model [24–26], the surface energy (γ) values of D18-Cl, Y6 and Y6-1O films are calculated to be 39.8, 43.9 and 43.2 mN m^{-1}, respectively. The similar γ values of 43.9 and 43.2 mN m^{-1}
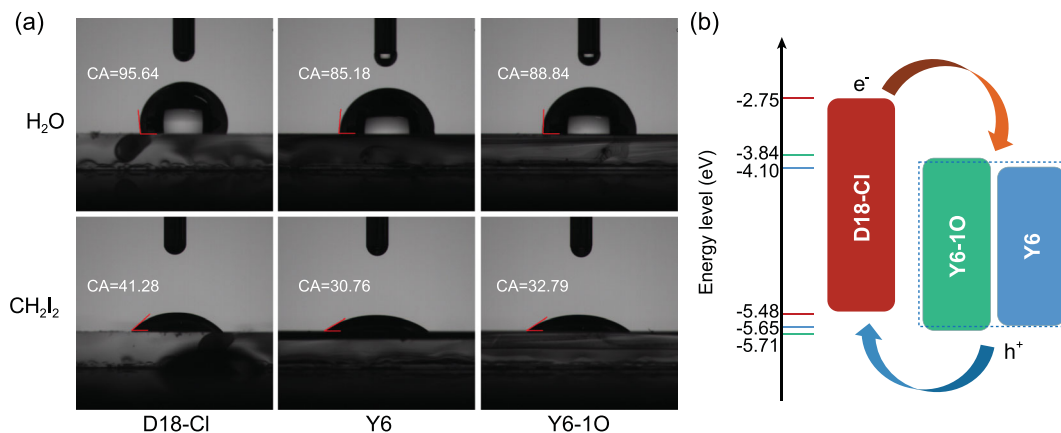
Figure 3. (a) The contact angle images of neat D18-Cl, Y6 and Y6-1O films. (b) Energy levels of used materials and diagram of alloy-like state.

indicate good compatibility between Y6 and Y6-1O. According to the γ values of neat films, the interfacial energy between two different materials can be calculated by employing the following equation:

$$\gamma_{X:Y} = \gamma_X + \gamma_Y - \frac{4\gamma_X^d \gamma_Y^d}{\gamma_X^d + \gamma_Y^d} - \frac{4\gamma_X^p \gamma_Y^p}{\gamma_X^p + \gamma_Y^p}.$$

Here, $\gamma_{X:Y}$ represents the interfacial energy between material X and Y; γ_X and γ_Y represent the surface energy of the neat materials; and superscript d and p are the dispersion and polar components calculated according to the contact angles, respectively [27]. The interfacial energy between Y6 and Y6-1O is calculated to be 0.16 mN m^{-1}, which is much lower than that ($\gamma_{D18-X:Y6} = 0.68$ mN m^{-1}, $\gamma_{D18-X:Y6-X} = 1.37$ mN m^{-1}) between donor and acceptor. The excellent compatibility between Y6 and Y6-1O can be firmly confirmed by the rather low interfacial energy, which is conducive to forming an alloy state of Y6 : Y6-1O. To further investigate the intermolecular interaction between Y6 and Y6-1O, photoluminescence (PL) spectra of Y6, Y6-1O and their blend films were measured and are shown in Fig. S3a. It is apparent that the PL emission peaks of blend films are gradually shifted from 860 to 850 nm along with the increase of Y6-1O content. Meanwhile, the PL emission intensity of the blend films is monotonously increased along with Y6-1O incorporation, suggesting the negligible charge and energy transfer between Y6 and Y6-1O. To further demonstrate the negligible charge transfer between two acceptors, a series of cells were fabricated with Y6, Y6-1O and Y6 : Y6-1O as active layers. The $J - V$ curves of the cells were measured under AM 1.5G illumination with light intensity of 100 mW cm^{-2} and are shown in Fig. S3b. The J_{SC} of Y6 : Y6-1O-based cells is in between that of Y6-based and Y6-1O-based cells, suggesting the negligible charge transfer or exciton dissociation at Y6 and Y6-1O interfaces. According to the above analysis, the dynamic processes in ternary OPVs can be schematically depicted in Fig. 3b. The photogenerated holes will be transported along the channels formed by D18-Cl, and the photogenerated electrons will be transported along the channels formed by Y6 : Y6-1O. The bi-continuous charge transport channels should be well formed in ternary active layers, resulting in over 76% FF for all ternary OPVs.

To investigate charge generation and exciton dissociation properties in active layers, photocurrent density (J_{ph}) versus effective voltage (V_{eff}) characteristics of typical OPVs were measured and are shown in Fig. 4a. Assuming that all photogenerated excitons are dissociated into free charges and then swept out under relatively large V_{eff} conditions, the J_{ph} can be defined as the saturated photocurrent density (J_{sat}) [28–31]. The J_{sat} values are 26.78, 26.92 and 23.96 mA cm^{-2} for D18-Cl : Y6 binary, optimal ternary and D18-Cl : Y6-1O binary OPVs. The relatively large J_{sat} value of the optimal ternary OPVs indicates improved photogenerated exciton density in ternary active layers. The exciton dissociation efficiency and charge collection efficiency can be evaluated according to J_{ph}^*/J_{sat} and $J_{ph}^\#/J_{sat}$, respectively. Here, J_{ph}^* and $J_{ph}^\#$ represent the J_{ph} values under short-circuit and maximal power output conditions, respectively. The J_{ph}^*/J_{sat} and $J_{ph}^\#/J_{sat}$ values of OPVs are increased to 96.1% and 86.5%, respectively, by incorporating 30 wt% Y6-1O in acceptors. The increased J_{ph}^*/J_{sat} and $J_{ph}^\#/J_{sat}$ values of ternary OPVs suggest that the phase separation of active layers can be well optimized by incorporating appropriate Y6-1O as morphology regulator, leading to improved FF of 76.92% for the optimal ternary OPVs. The detailed J_{ph} values of typical OPVs at different conditions are summarized in Table S2. To gain more insight into the charge separation process
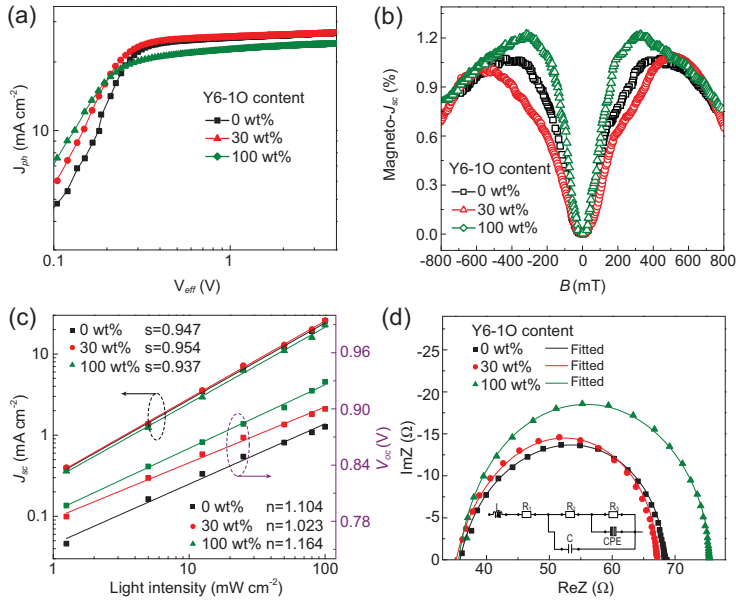
Figure 4. (a) $J_{ph} - V_{eff}$ curves of typical OPVs. (b) Magneto-photocurrent curves of typical OPVs under 635 nm photo-excitation. (c) $J_{SC} - P_{light}$ and $V_{OC} - P_{light}$ curves of typical OPVs. (d) Impedance spectra responses of corresponding OPVs; the inset represents the equivalent circuit model.

in distinct active layers, the magneto-photocurrent (magneto-J_{SC}) characteristics of typical OPVs were investigated. The magneto-J_{sc} was employed to monitor the charge separation at donor–acceptor interfaces based on the following processes. The singlet excitons are generated due to the spin selection rule under photoexcitation. Singlet excitons can migrate to the donor–acceptor interface to produce electron-hole pairs. The electron-hole pairs can be partially converted into triplet polaron pairs through intersystem crossing caused by internal magnetic interaction such as hyperfine interaction and spin-orbital coupling, leading to coexistence of singlet and triplet electron-hole pairs. The populations of singlet and triplet electron-hole pairs can be changed with the application of magnetic field through intersystem crossing, leading to a varied photocurrent due to different dissociation rates of singlets and triplets. The magneto-J_{SC} of OPVs is firmly related to the ratio of spin-related singlet state and triplet state forming at donor–acceptor interfaces. The magneto-J_{SC} was recorded by measuring the photocurrent of OPVs as a function of magnetic field under the 635 nm photoexcitation condition, as shown in Fig. 4b. The magneto-J_{SC} can be calculated according to the following equation:

$$\text{magneto-}J_{SC} = \frac{I(B) - I(0)}{I(0)} \times 100\%.$$

Here, $I(B)$ and $I(0)$ represent the photocurrent measured with and without a magnetic field, respec-

tively [32,33]. As shown in Fig. 4b, the optimal binary and ternary OPVs show a positive magneto-J_{SC} signal within the sweeping fields $\pm$ 800 mT, which should be ascribed to the increased singlet/triplet ratio under a magnetic field. In comparison with binary OPVs, the optimal ternary OPVs exhibit the relatively small magnitude of magneto-J_{SC} at low magnetic field strength. The relatively small magneto-J_{SC} of the optimal ternary OPVs suggests more efficient charge separation in ternary active layers, which can well support the increased J_{SC} of the optimal ternary OPVs.

To understand the charge recombination process in active layers, $J - V$ curves of typical OPVs were measured under different light intensity, as shown in Fig. S4. Based on the $J - V$ curves, J_{SC} and V_{OC} of typical OPVs versus the incident intensity (P_{light}) were plotted as shown in Fig. 4c. The relationship between J_{SC} and P_{light} can be described as $J_{SC} \propto P_{light}^{s}$ [34–37]. The power-law exponential factor s represents the degree of bimolecular recombination, which should be equal to 1 if the bimolecular recombination is completely suppressed. The fitted s values are 0.947, 0.954 and 0.937 for D18-Cl : Y6 binary, optimal ternary and D18-Cl : Y6-1O binary OPVs. The fitted s value of the optimal ternary OPVs is much closer to 1, indicating that the bimolecular recombination in active layers can be effectively restrained with appropriate Y6-1O incorporation. The degree of trap-assisted recombination in OPVs can be evaluated by applying the equation $V_{OC} \propto n(KT/q)\ln P_{light}$, in which K, T and q represent the Boltzmann constant, absolute temperature and elementary charge, respectively [38–41]. The trap-assisted recombination in active layers should be negligible with the slope close to KT/q. The slope is decreased from 1.104 KT/q (D18-Cl : Y6 binary OPVs) or 1.164 KT/q (D18-Cl : Y6-1O binary OPVs) to 1.023 KT/q for the optimal ternary OPVs, indicating that trap-assisted recombination can be suppressed by incorporating appropriate Y6-1O. The synchronously mitigated bimolecular and trap-assisted recombination of the optimal ternary active layers is conducive to efficient charge transport and collection, leading to improved FF of 76.92% for the optimal ternary OPVs.

To gain more insight into the effect of incorporating Y6-1O into the charge transport and recombination process, the impedance spectroscopy (IS) measurements were carried out in frequency range from 20 Hz to 3.5 MHz. Figure 4d exhibits the Nyquist plots of the typical binary and ternary OPVs measured at V = V_{OC}. The equivalent circuit model used to fit Nyquist plots data are shown in the inset of Fig. 4d. In this model, the inductance (L) was

employed to eliminate the impact of the connecting wires during high-frequency scans; R_1 represents the series resistance deriving from electrodes and bulk resistance in active layers; and R_2 and R_3 represent transport and recombination resistance in active layers, respectively [42]. The capacitor (C) accounts for the dielectric behavior of OPVs. The constant phase element (CPE) is introduced to the circuit model, which indicates non-ideal behavior of the capacitor. The CPE is defined by the equation $Z = (CPE_T)^{-1}(iw)^{CPE_P}$, in which w is the angular frequency, and CPE_T and CPE_P represent capacitance and inhomogeneous constant, respectively [43,44]. If CPE_P is equal to 1, the CPE is identical to an ideal capacitor without the presence of any defects at the interface between donor and acceptor [45]. The fitted parameters of typical OPVs are summarized in Table S3. The R_2 values are decreased from 23.2 (D18-Cl : Y6 binary OPVs) or 32.3 (D18-Cl : Y6-1O binary OPVs) to 18.1 Ω for the optimal ternary OPVs, while the R_3 values are increased from 11.3 (D18-Cl : Y6 binary OPVs) or 9.29 (D18-Cl : Y6-1O binary OPVs) to 16.2 Ω for the optimal ternary OPVs. The smaller R_2 and larger R_3 values of the optimal ternary OPVs should facilitate charge transport and restrain charge recombination in ternary active layers, leading to improved FF for the optimal ternary OPVs. The CPE_P values are 0.941, 0.977 and 0.956 for D18-Cl : Y6 binary, optimal ternary and D18-Cl : Y6-1O binary OPVs, respectively. In comparison with two binary OPVs, the CPE_P of the optimal ternary OPVs is much closer to 1, indicating that the interfacial capacitance is more electrically ideal by incorporating appropriate Y6-1O.

The charge mobility in blend films were characterized based on the space charge limited current (SCLC) method. The configurations of hole-only and electron-only devices are described in the Supporting Information. The $\ln(Jd^3/V^2)$-$(V/d)^{0.5}$ curves of hole-only and electron-only devices are depicted in Fig. S5. The hole mobility (μ_h) and electron mobility (μ_e) of blend films are increased to 8.67×10^{-4} cm^2 V^{-1} s^{-1} and 6.06×10^{-4} cm^2 V^{-1} s^{-1} by incorporating 30 wt% Y6-1O in acceptors, indicating that a more efficient charge transport channel should be formed in the optimal ternary active layers. The μ_h/μ_e values can be employed to estimate charge transport balance in active layers [46–49]. The μ_h/μ_e values are 1.63, 1.43 and 1.70 for D18-Cl : Y6 binary, optimal ternary and D18-Cl : Y6-1O binary OPVs. The μ_h/μ_e value of optimal ternary OPVs is closest to 1, indicating a more balanced charge transport in the optimal ternary active layers. The increased charge mobility and more balanced charge transport can rationalize the relatively high FF of 76.92% in the

optimal ternary OPVs. The detailed μ_h, μ_e, and μ_h/μ_e of the corresponding devices are summarized in Table S2. It is well known that charge transport is closely related to the molecular packing property of blend films. The grazing-incidence wide-angle X-ray scattering (GIWAXS) characterization was performed to investigate the effect of Y6-1O content on molecular arrangement.

The 2D GIWAXS patterns and the corresponding out-of-plane (OOP) and in-plane (IP) profiles of neat D18-Cl, Y6 and Y6-1O films are shown in Fig. S6. The neat Y6 and Y6-1O films exhibit relatively apparent OOP (010) and IP (100) diffraction peaks, suggesting preferential face-on orientation with respect to the substrates. Except for the OOP (010) and IP (100) diffraction peaks, neat D18-Cl films also show relatively apparent OOP (100) diffraction peak, signifying the coexistence of face-on and edge-on orientation with respect to the substrates. The 2D GIWAXS patterns and the corresponding OOP and IP profiles of blend films are shown in Fig. 5a and b, respectively. Upon blending D18-Cl with Y6 or Y6-1O, the resultant blend films exhibit a preferential face-on orientation, which is evidenced by the pronounced OOP (010) and IP (100) diffraction peaks. The OOP (010) diffraction peaks of binary blend films are located at the same positions as in their corresponding neat acceptor films, suggesting that the π–π stacking in blend films is dominated by acceptors. The IP (100) diffraction peaks of blend films are located at 0.31 Å^{-1}, which should be mainly attributed to the ordered lamellar stacking of D18-Cl, as confirmed by the relatively strong IP (100) diffraction peak of neat D18-Cl film. For the optimal ternary blend films, the OOP (010) and IP (100) diffraction peaks are simultaneously improved in comparison with those of two binary blend films, suggesting more ordered face-on orientation in the optimal ternary blend films. The π–π stacking distance in the optimal ternary blend films is calculated to be 3.67 Å, which is slightly shorter than that of D18-Cl : Y6-based blend films. The reduction of the intermolecular π–π stacking distance in OOP direction should promote the electron transport in ternary active layers. The molecular correlation length (L_C) can be evaluated according to the equation $L_C = 2\pi k/f_{whm}$, where k is the shape factor typically with the value of 0.9, and f_{whm} is the full-width at half-maximum of a diffraction peak [50]. In the optimal ternary blend films, the L_C related to lamellar stacking is calculated to be 5.8 nm, which is larger than that of binary blend films. The increased L_C in ternary blend films corresponds to the higher D18-Cl domain crystallinity. In comparison with binary blend films, the quite different IP (100) diffraction peak in ternary blend films should
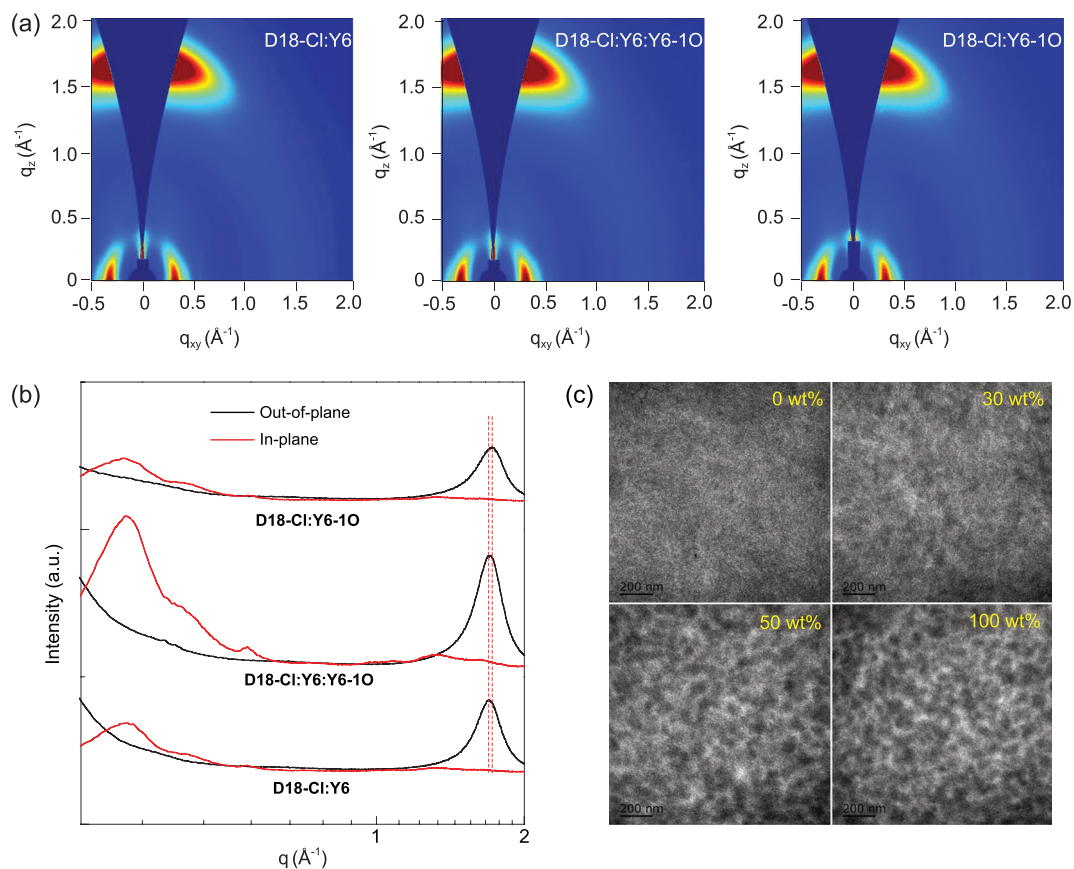
Figure 5. (a) The 2D-GIWAXS patterns of corresponding blend films. (b) The out-of-plane (black line) and in-plane (red line) line-cut profiles of the GIWAXS patterns in blend films. (c) TEM images of blend films with distinct Y6-1O content.

originate from more ordered lamellar stacking and higher crystallinity of D18-Cl. The more ordered molecular arrangement of D18-Cl should facilitate hole transport, leading to increased hole mobility of ternary active layers. The detailed vector values of diffraction peaks and L_C values in neat and blend films are summarized in Table S4.

To unveil the effect of the Y6-1O content on the bulk morphology of blend films, transmission electron microscopy (TEM) was carried out on the blend films, as shown in Fig. 5c. The homogeneous and nanofibrous structures can be observed from the TEM images of Y6-based binary blend films. The island-like structure with a relatively large phase separation degree can be observed from the TEM images of Y6-1O-based binary blend films, which can be well explained by the relatively large interfacial energy between D18-Cl and Y6-1O. As observed from the TEM images of ternary blend films, the aggregated structure between donor and acceptor, as well as the phase separation degree are gradually varied along with the incorporation of Y6-1O. The gradually varied morphology of ternary blend films depending on Y6-1O content suggests that Y6-1O can act as morphology regulator. The appropriate phase

separation degree should be formed in the optimal ternary active layers, which provide enough donor–acceptor interfacial area for exciton dissociation, as well as a bi-continuous percolating charge transport path to electrodes.

CONCLUSION

The PCE of 17.07% is achieved in D18-Cl : Y6-based OPVs. On this basis, a series of ternary OPVs are fabricated by employing Y6-1O as the third component. The 17.91% PCE is achieved in the optimal ternary OPVs with 30 wt% Y6-1O in acceptors, which should be among the highest levels in ternary OPVs. The photon harvesting, molecular arrangement and phase separation degree in active layers can be finely adjusted by incorporating appropriate Y6-1O, leading to the synchronously improved J_{SC} and FF of ternary OPVs. The improved phase separation and molecular arrangement are beneficial to efficient charge separation and transport in ternary active layers, which can be confirmed by the experimental results of GIWAXS and TEM. The more efficient charge separation and transport processes in ternary active layers can be well explained

by the magneto-J_{SC} and IS measurement results. Meanwhile, the E_{loss} of ternary OPVs is gradually decreased along with the incorporation of Y6-1O, leading to improved V_{OC} in ternary OPVs. This work delivers more insight into the potential reasons for the third component's effect on performance improvement of ternary OPVs.

SUPPLEMENTARY DATA

Supplementary data are available at NSR online.

AUTHOR CONTRIBUTIONS

X. Ma carried out the device fabrication and characterization. A. Zeng and H. Yan synthesized the materials D18-Cl and Y6-1O. F. Zhang, X. Ma and Y. Wang designed the experiments and finished the manuscript writing. J. Gao, Z. Hu and C. Xu also took part in the experimental details. X. Ma, J. Son, S. Jeong and H. Woo carried out the GIWAXS experiment. X. Ma, C. Zhang and K. Wang finished the magneto-J_{SC} data measurement and analysis. X. Ma, M. Li and Z. Ma carried out the s-EQE, EL and EQE_{EL} spectra of OPVs. All authors discussed and commented on the paper.

Conflict of interest statement. None declared.

REFERENCES

1. Yao J, Qiu B and Zhang Z *et al.* Cathode engineering with perylene-diimide interlayer enabling over 17% efficiency single-junction organic solar cells. *Nat Commun* 2020; **11**: 2726.
2. Cui Y, Yao H and Zhang J *et al.* Single-junction organic photovoltaic cells with approaching 18% efficiency. *Adv Mater* 2020; **32**: 1908205.
3. Lin F, Jiang K and Kaminsky W *et al.* A non-fullerene acceptor with enhanced intermolecular pi-core interaction for high-performance organic solar cells. *J Am Chem Soc* 2020; **142**: 15246–51.
4. Cui Y, Yao H and Hong L *et al.* Organic photovoltaic cell with 17% efficiency and superior processability. *Natl Sci Rev* 2020; **7**: 1239–46.
5. Xiao Z, Jia X and Ding L. Ternary organic solar cells offer 14% power conversion efficiency. *Sci Bull* 2017; **62**: 1562–4.
6. Gao J, Gao W and Ma X *et al.* Over 14.5% efficiency and 71.6% fill factor of ternary organic solar cells with 300 nm thick active layers. *Energy Environ Sci* 2020; **13**: 958–67.
7. Su W, Fan Q and Guo X *et al.* Two compatible nonfullerene acceptors with similar structures as alloy for efficient ternary polymer solar cells. *Nano Energy* 2017; **38**: 510–7.
8. Ma X, Wang J and Gao J *et al.* Achieving 17.4% efficiency of ternary organic photovoltaics with two well-compatible non-fullerene acceptors for minimizing energy loss. *Adv Energy Mater* 2020; **10**: 2001404.
9. Zhou Z, Xu S and Song J *et al.* High-efficiency small-molecule ternary solar cells with a hierarchical morphology enabled by synergizing fullerene and non-fullerene acceptors. *Nat Energy* 2018; **3**: 952–9.
10. Yu R, Yao H and Cui Y *et al.* Improved charge transport and reduced nonradiative energy loss enable over 16% efficiency in ternary polymer solar cells. *Adv Mater* 2019; **31**: 1902302.
11. Ma X, Wang J and An Q *et al.* Highly efficient quaternary organic photovoltaics by optimizing photogenerated exciton distribution and active layer morphology. *Nano Energy* 2020; **70**: 104496.
12. Liu T, Luo Z and Fan Q *et al.* Use of two structurally similar small molecular acceptors enabling ternary organic solar cells with high efficiencies and fill factors. *Energy Environ Sci* 2018; **11**: 3275–82.
13. Wang X, Sun Q and Gao J *et al.* Ternary organic photovoltaic cells exhibiting 17.59% efficiency with two compatible Y6 derivations as acceptor. *Sol RRL* 2021; doi: 10.1002/solr.202100007.
14. An Q, Wang J and Ma X *et al.* Two compatible polymer donors contribute synergistically for ternary organic solar cells with 17.53% efficiency. *Energy Environ Sci* 2020; **13**: 5039–47.
15. Yuan J, Zhang Y and Zhou L *et al.* Single-junction organic solar cell with over 15% efficiency using fused-ring acceptor with electron-deficient core. *Joule* 2019; **3**: 1140–51.
16. Liu Q, Jiang Y and Jin K *et al.* 18% efficiency organic solar cells. *Sci Bull* 2020; **65**: 272–5.
17. Xu X, Feng K and Lee Y *et al.* Subtle polymer donor and molecular acceptor design enable efficient polymer solar cells with a very small energy loss. *Adv Funct Mater* 2020; **30**: 1907570.
18. Hong L, Yao H and Wu Z *et al.* Eco-compatible solvent-processed organic photovoltaic cells with over 16% efficiency. *Adv Mater* 2019; **31**: 1903441.
19. An Q, Gao W and Zhang F *et al.* Energy level modulation of non-fullerene acceptors enables efficient organic solar cells with small energy loss. *J Mater Chem A* 2018; **6**: 2468–75.
20. Menke S, Ran N and Bazan G *et al.* Understanding energy loss in organic solar cells: toward a new efficiency regime. *Joule* 2018; **2**: 25–35.
21. Azzouzi M, Yan J and Kirchartz T *et al.* Nonradiative energy losses in bulk-heterojunction organic photovoltaics. *Phys Rev X* 2018; **8**: 031055.
22. Zhan L, Li S and Lau T *et al.* Over 17% efficiency ternary organic solar cells enabled by two non-fullerene acceptors working in an alloy-like model. *Energy Environ Sci* 2020; **13**: 635–45.
23. Chen Y, Ye P and Zhu Z *et al.* Achieving high-performance ternary organic solar cells through tuning acceptor alloy. *Adv Mater* 2017; **29**: 1603154.
24. Comyn J. Contact angles and adhesive bonding. *Int J of Adhes Adhes* 1992; **12**: 145–9.

25. Jiang K, Zhang G and Yang G *et al.* Multiple cases of efficient nonfullerene ternary organic solar cells enabled by an effective morphology control method. *Adv Energy Mater* 2018; **8**: 1701370.

26. Hu Z, Yang L and Gao W *et al.* Over 15.7% efficiency of ternary organic solar cells by employing two compatible acceptors with similar LUMO levels. *Small* 2020; **16**: 2000441.

27. Song J, Li C and Zhu L *et al.* Ternary organic solar cells with efficiency >16.5% based on two compatible nonfullerene acceptors. *Adv Mater* 2019; **31**: 1905645.

28. Ma Y, Cai D and Wan S *et al.* Ladder-type heteroheptacenes with different heterocycles for nonfullerene acceptors. *Angew Chem Int Edit* 2020; **59**: 21627–33.

29. Liu L, Kan Y and Gao K *et al.* Graphdiyne derivative as multifunctional solid additive in binary organic solar cells with 17.3% efficiency and high reproductivity. *Adv Mater* 2020; **32**: 1907604.

30. An Q, Zhang F and Gao W *et al.* High-efficiency and air stable fullerene-free ternary organic solar cells. *Nano Energy* 2018; **45**: 177–83.

31. Zhao Z, Xu C and Niu L *et al.* Recent progress on broadband organic photodetectors and their applications. *Laser Photonics Rev* 2020; **14**: 2000262.

32. Zhang C, Wang K and Zhao F *et al.* Essential relation of spin states, trap states and photo-induced polarization for efficient charge dissociation in a polymer-nonfullerene based organic photovoltaic system. *Nano Energy* 2020; **78**: 105324.

33. Zhu X, Zhang G and Zhang J *et al.* Self-stimulated dissociation in non-fullerene organic bulk-heterojunction solar cells. *Joule* 2020; **4**: 2443–57.

34. Ma Q, Jia Z and Meng L *et al.* Promoting charge separation resulting in ternary organic solar cells efficiency over 17.5%. *Nano Energy* 2020; **78**: 105272.

35. Hu Z, Zhang F and An Q *et al.* Ternary nonfullerene polymer solar cells with a power conversion efficiency of 11.6% by inheriting the advantages of binary cells. *ACS Energy Lett* 2018; **3**: 555–61.

36. Lin Y, Firdaus Y and Nugraha M *et al.* 17.1% efficient single-junction organic solar cells enabled by n-type doping of the bulk-heterojunction. *Adv Sci* 2020; **7**: 1903419.

37. Gao J, Wang J and An Q *et al.* Over 16.7% efficiency of ternary organic photovoltaics by employing extra PC$_{71}$BM as morphology regulator. *Sci Chi Chem* 2020; **63**: 83–91.

38. Hu Z, Wang J and Ma X *et al.* A critical review on semitransparent organic solar cells. *Nano Energy* 2020; **78**: 105376.

39. Li K, Wu Y and Tang Y *et al.* Ternary blended fullerene-free polymer solar cells with 16.5% efficiency enabled with a higher-LUMO-level acceptor to improve film morphology. *Adv Energy Mater* 2019; **9**: 1901728.

40. Wang X, Du Z and Dou K *et al.* A maverick asymmetrical backbone with distinct flanked twist angles modulating the molecular aggregation and crystallinity for high performance nonfullerene solar cells. *Adv Energy Mater* 2019; **9**: 1802530.

41. Ma X, An Q and Ibraikulov OA *et al.* Efficient ternary organic photovoltaics with two polymer donors by minimizing energy loss. *J Mater Chem A* 2020; **8**: 1265–72.

42. Wei L, Cai J and Cai F *et al.* Achieving over 11% power conversion efficiency in PffBT4T-2OD-based ternary polymer solar cells with enhanced open-circuit-voltage and suppressed charge recombination. *Nano Energy* 2018; **44**: 155–63.

43. Perrier G, Bettignies R and Berson S *et al.* Impedance spectrometry of optimized standard and inverted P3HT-PCBM organic solar cells. *Sol Energy Mat Sol C* 2012; **101**: 210–6.

44. Xu C, Chen H and Zhao Z *et al.* 14.46% efficiency small molecule organic photovoltaics enabled by the well trade-off between phase separation and photon harvesting. *J Energy Chem* 2021; **57**: 610–7.

45. Sacco A. Electrochemical impedance spectroscopy: fundamentals and application in dye-sensitized solar cells. *Renew Sust Energy Rev* 2017; **79**: 814–29.

46. Luo Z, Sun R and Zhong C *et al.* Altering alkyl-chains branching positions for boosting the performance of small-molecule acceptors for highly efficient nonfullerene organic solar cells. *Sci Chi Chem* 2020; **63**: 361–9.

47. Gao J, Wang J and Xu C *et al.* A critical review on efficient thick-film organic solar cells. *Solar RRL* 2020; **4**: 2000364.

48. Ma X, Luo M and Gao W *et al.* Achieving 14.11% efficiency of ternary polymer solar cells by simultaneously optimizing photon harvesting and exciton distribution. *J Mater Chem A* 2019; **7**: 7843–51.

49. Ma Y, Cai D and Wan S *et al.* Control over $\pi-\pi$ stacking of heteroheptacene-based nonfullerene acceptors for 16% efficiency polymer solar cells. *Natl Sci Rev* 2020; **7**: 1886–95.

50. Du X, Yuan Y and Zhou L *et al.* Delayed fluorescence emitter enables near 17% efficiency ternary organic solar cells with enhanced storage stability and reduced recombination energy loss. *Adv Funct Mater* 2020; **30**: 1909837.